NIH Public Access
Author Manuscript
Nanomedicine (Lond). Author manuscript; available in PMC 2014 April 18.

Published in final edited form as:
Nanomedicine (Lond). 2012 November ; 7(11): 1697–1711. doi:10.2217/nnm.12.65.

Preliminary study of injury from heating systemically delivered, nontargeted dextran–superparamagnetic iron oxide nanoparticles in mice

Carmen Kut[1], **Yonggang Zhang**[1], **Mohammad Hedayati**[1], **Haoming Zhou**[1], **Christine Cornejo**[1], **David Bordelon**[1], **Jana Mihalic**[2], **Michele Wabler**[1], **Elizabeth Burghardt**[1], **Cordula Gruettner**[3], **Alison Geyh**[2], **Cory Brayton**[1], **Theodore L Deweese**[1], and **Robert Ivkov**[*,1]

[1]Johns Hopkins University School of Medicine, 1550 Orleans Street, CRB I, Baltimore, MD 21231, USA

[2]Department of Environmental Health Sciences, Johns Hopkins Bloomberg School of Public Health, Baltimore, MD 21205, USA

[3]Micromod Partikeltechnologie GmbH, Friedrich-Barnewitz-St 4, D-18119 Rostock, Germany

Abstract

Aim—To assess the potential for injury to normal tissues in mice due to heating systemically delivered magnetic nanoparticles in an alternating magnetic field (AMF).

Materials & methods—Twenty three male nude mice received intravenous injections of dextran–superparamagnetic iron oxide nanoparticles on days 1–3. On day 6, they were exposed to AMF. On day 7, blood, liver and spleen were harvested and analyzed.

Results—Iron deposits were detected in the liver and spleen. Mice that had received a high-particle dose and a high AMF experienced increased mortality, elevated liver enzymes and significant liver and spleen necrosis. Mice treated with low-dose superparamagnetic iron oxide nanoparticles and a low AMF survived, but had elevated enzyme levels and local necrosis in the spleen.

Conclusion—Magnetic nanoparticles producing only modest heat output can cause damage, and even death, when sequestered in sufficient concentrations. Dextran–superparamagnetic iron oxide nanoparticles are deposited in the liver and spleen, making these the sites of potential toxicity.

© 2012 Future Medicine Ltd

[*]Author for correspondence: Tel.: +1 443 287 7282, Fax: +1 410 502 2821, rivkov1@jhmi.edu.

Financial & competing interests disclosure
The authors have no other relevant affiliations or financial involvement with any organization or entity with a financial interest in or financial conflict with the subject matter or materials discussed in the manuscript apart from those disclosed.
No writing assistance was utilized in the production of this manuscript.

Ethical conduct of research
The authors state that they have obtained appropriate institutional review board approval or have followed the principles outlined in the Declaration of Helsinki for all human or animal experimental investigations. In addition, for investigations involving human subjects, informed consent has been obtained from the participants involved.

NIH-PA Author Manuscript
NIH-PA Author Manuscript
NIH-PA Author Manuscript

NIH-PA Author Manuscript

NIH-PA Author Manuscript

NIH-PA Author Manuscript

Keywords

hyperthermia; liver; magnetic nanoparticle; SPIO; spleen; toxicity

Metastatic cancer is often refractory to standard therapies such as radiation and certain chemotherapeutic agents. Heat potently sensitizes cancer cells to such therapies [1–5], and multimodality treatments that have integrated therapeutic heating have been successfully used for some primary cancers in Phase II/III randomized clinical trials. However, heat-based therapies remain on the periphery of clinical oncology [6–11], except in specific cases (e.g., cervical cancer) [11]. The main barrier for the clinical translation of these therapies is the technical difficulty in effectively heating multiple metastatic lesions without damaging critical nondiseased tissues [1].

Magnetic iron oxide nanoparticles targeted to specific markers on cancer cells have recently emerged as a promising technology for delivering cell-specific heat [12–22] and as potential platforms to provide both imaging and therapy [18]. These particles generate heat when subjected to an external alternating magnetic field (AMF) [16,23,24]. Animal studies have demonstrated the potential for successful therapy following systemic or intravenous (iv.) delivery of nanoparticles labeled with antibodies that bind specifically to cancer cells [24,25].

These studies have demonstrated, however, that dextran–iron oxide nanoparticles with a mean diameter >20 nm accumulate mostly in the liver and spleen, with a fraction entering the tumor – the intended therapeutic target. For some superparamagnetic iron oxide (SPIO) nanoparticles, deposition in the liver and spleen is acceptable. The first-generation SPIO MRI contrast agent, Feridex I.V.® (AMAG Pharmaceuticals, MA, USA), intended for use as a liver cancer imaging agent, is typically given at low doses [26], clears rapidly from the body [27] and produces no heat [28]. Thus the high deposition of Feridex in the liver and spleen (85–95% of an injected dose) has been considered clinically irrelevant [29]. New-generation nanoparticles, on the other hand, are intended for use as hyperthermia-inducing agents and, as such, were designed to require high-dose injections, clear more slowly from the body and heat maximally [14,25]. Consequently, it is important to assess their potential ability to inadvertently damage normal organs. Such an understanding would help clinicians to make informed decisions about continued development and clinical translation of magnetically induced hyperthermia-based therapies for cancer.

Active ‘targeting’ of nanoparticles may ineffectively impair the interactions of the nanoparticles with the untargeted tissues and organs of the host [30], and thus concerns about the presence of nanoparticles and consequent toxicity in these organs remain to be addressed [31–34]. Immediately following injection into the blood, nanoparticles (even targeted ones) interact with blood components (i.e., proteins, membranes, cells and DNA), leading to the formation of a protein ‘corona’ on the nanoparticles [31]. This protein corona directs nanoparticle complexes to their ultimate sites of deposition [31,32,34], largely through the fixed macrophages of the reticuloendothelial system [31]. The toxicological impact of the deposition and presence of nanoparticles, such as those developed for MRI contrast, in organs and tissues has been characterized. It is commonly observed that these

NIH-PA Author Manuscript

NIH-PA Author Manuscript

NIH-PA Author Manuscript

particles localize primarily to the liver and spleen where they may be degraded, leading to concerns that the interaction of cells with materials comprising of the nanoparticles or their degradation products may lead to adverse effects in patients. To date, little effort has been devoted to understanding the toxicity that may result from heating deposits of poorly targeted nanoparticles, even those having formulations that potently deliver heat. In this pilot study, the authors obtained initial data concerning the distribution and extent of damage after nonspecific, systemic delivery of a single dextran–iron oxide magnetic nanoparticle formulation and subsequent heating by AMF in order to motivate further study of the potential toxic effects of inadvertent heating of magnetic nanoparticles. The authors evaluated such potential damage by iv. injection of SPIO nanoparticles into nude mice and then exposing these mice to an AMF (0, 24 and 60 kA/m).

Tissue heating with magnetic nanoparticles that are excited by an AMF is certainly well known. Proposed strategies to exploit this combination using systemically delivered, molecular-targeted nanoparticles typically ignore the full consequences of heating organs, such as the liver and spleen, which sequester the vast majority of the particles [12,25,30]. To the author's knowledge, nonspecific uptake of nanoparticles by the liver and spleen, and any subsequent potential for organ damage when these particles are heated in an AMF, have not been experimentally addressed. This represents a potential gap in SPIO nanoparticle toxicity research, which has focused primarily on material-related cytotoxicity, protein–nanoparticle interactions, and its effect on cell- and tissue-specific inflammation processes [31–34]. This study therefore intends to highlight the potential for gross thermal toxicity in the liver and spleen, and provide preliminary data that may guide future preclinical experimental designs. It also serves as a reminder that the pursuit of increasingly potent (heat-generating) nanoparticle formulations without a concomitant improvement in selective targeting will probably lead to increased acute thermal toxicity.

Materials & methods

Experimental design

Twenty three nude mice received daily iv. retro-orbital injections of magnetic dextran–iron oxide nanoparticles (NanoMAG™-D-SPIO; hereafter referred to as SPIO nanoparticles [micromod Partikeltechnologie GmbH, Rostock, Germany]: zero-, low- or high-dose) on days 1–3 and were exposed to an AMF field (zero-, low- or high-field strength) on day 6. Blood was collected and organs were harvested after euthanasia on day 7 (Figure 1A).

Mice were assigned to one of seven groups, of three or four mice per group (Figure 1B), including three control groups (S0, SH and H0) and four treatment groups (LL, LH, HL and HH). The first letter of each group designation indicates the dose of nanoparticles injected: saline (S), low-dose SPIO (L) or high-dose SPIO (H). The second letter of each group designation indicates the field strength for AMF exposure: zero-(0), low- (L) or high-field (H).

NIH-PA Author Manuscript

NIH-PA Author Manuscript

NIH-PA Author Manuscript

Mice

Male nude mice (Hsd: Athymic Nude-Foxn1^{nu}, Harlan Labs, IN, USA) were used in this study. All mice were 5–7 weeks old and weighed 17–31 g prior to treatment. Mice were housed in an Association for Assessment and Accreditation of Laboratory Animal Care-accredited facility in compliance with the Guide for the Care and Use of Laboratory Animals [35], and procedures were approved by the Johns Hopkins Institutional Animal Care and Use Committee. Male nude mice were selected for their relevance to the authors' ongoing studies on prostate cancer therapy.

Nanoparticles

Suspensions of 100-nm dextran–iron oxide particles (NanoMAG-D-SPIO) in water were purchased from micromod Partikeltechnologie, GmbH (Rostock, Germany). These nanoparticles were produced by precipitating ferric and ferrous chlorides from solution in the presence of dextran [36]. The measured iron content was <40% w/w, with a total iron concentration of 6 mg/ml [37]. The SPIO nanoparticles comprised of magnetite crystals, Fe_3O_4, which had a mean diameter of 10–12 nm [38], and were embedded in a dextran matrix. The particles were suspended in sterile water to provide a stable biocompatible suspension [36,38].

Size measurements were performed on the samples by photon correlation spectroscopy using a Malvern Zetasizer Nano ZS-90 (Malvern Instruments Ltd, Worcestershire, UK) at an iron concentration of 0.4 mg/ml in 0.22-μm-filtered water (z-weighted distribution) (Figure 2A). ζ-potential–pH function of the nanoparticles was measured using the same system and indicated a slightly negatively charged surface over pH 3–10 and a surface charge of approximately −6 mV at approximately pH 7 (Figure 2B).

Transmission electron microscopy images were obtained using an EM 912 transmission electron microscope (Zeiss, Oberkochen, Germany) at 100 keV. Analysis of the transmission electron microscopy images suggests that the SPIO nanoparticles comprise of well-adhered, multiple crystalline domains (Figure 2C). The dextran coating is typically not visible with high-energy electrons (100 keV); however, the proximity of the crystalline domains to one another suggests they were adherent and not merely agglomerated. Thus, the particle size inferred from analysis of the transmission electron microscopy images (50-nm diameter iron oxide core) generally agreed with the sizes obtained from photon correlation spectroscopy data (100-nm diameter, including both iron oxide core and dextran coating), with a small polydispersity index value indicating a narrow size distribution.

AMF system

The AMF system has been previously described [39,40]. This system comprises of three main components: the inductor coil, external capacitance network (Fluxtrol Inc., MI, USA), and an 80-kW power supply (PPECO, CA, USA). Together, the inductor coil (or inductor), external capacitance network and power supply form the resonant circuit.

Stable oscillation at 140–160 kHz was achieved with tune capacitors in the matchbox (Fluxtrol Inc.). The AMF system was calibrated using a field probe (Fluxtrol Inc.), as

NIH-PA Author Manuscript

NIH-PA Author Manuscript

NIH-PA Author Manuscript

previously described [36], and field amplitude was measured in the coil center before each trial. During operation, the inductor coil and all AMF components were cooled using a closed-loop, circulating water system maintained between 22 and 25°C (Dry Cooler Systems Inc., MI, USA).

In addition to minimizing nonspecific heating from eddy currents, an additional circulating water shield, inserted within the inducting coil, was designed to maintain a constant ambient temperature of 37°C [41].

Particle SLP measurements

The particle heating efficiency or specific loss power (SLP) was used to estimate the loss power heating during AMF exposure. While the SLP depends on the AMF amplitude and AMF frequency, the total heat delivered to a particular volume of tissue by the particles also depends upon the total particle concentration in that volume and on the total time of AMF exposure [24,25].

Methods and equipment used to characterize the SLP have been described in detail elsewhere [36] and are summarized below. The magneto-thermal set-up comprises of an insulating sample holder placed within a modified solenoid induction coil connected to the AMF system described above. The amplitude-dependent SLP for each particle was estimated from measured time-dependent heating at several applied amplitude (voltage) values from 4 to 94 kA/m. Sample temperatures were measured with fiber optic probes (FISO Technologies, Quebec City, Canada). The SLP was estimated from the slope, $\Delta T/\Delta t$, of the time–temperature curve (Figure 2D).

Nanoparticle injections & AMF treatment

On days 1–3, all mice received daily isoflurane (inhalation anesthesia) for retro-orbital injections. Control groups (S0, SH and H0) received three 0.4-ml daily injections of saline, mice in the high-dose treatment groups (HL and HH) received three 0.4-ml daily injections of SPIO nanoparticles (6 mg of iron/ml or 7.2 mg of iron per mouse), and mice in the low-dose treatment groups (LL and LH) received one 0.275-ml daily injection of SPIO nanoparticles (6 mg of iron/ml or 1.65 mg of iron per mouse). Each mouse was exposed to AMF 72 h after the third (final) nanoparticle injection.

For AMF exposure, each mouse was placed in a chamber constructed from a standard polypropylene 50-ml conical centrifuge tube that was positioned in the center of the solenoid coil. On day 6, mice in groups SH, HL, HH, LL and LH received intraperitoneal injections of ketamine/xylazine (anesthesia) at an approximate dose of 200 µl. Each mouse was placed in the coil for 30 min and exposed to one of the following AMF amplitudes: 0, 24 or 60 kA/m, corresponding to the 0, L or H designations, respectively (Figure 1B). During AMF exposure, mice were placed into the AMF inductor coil such that the abdominal region of each mouse was positioned in the center of the coil and therefore exposed to the maximum magnetic field, corresponding to the measured (by field probe) field. Rectal temperatures were measured at 1 s intervals for each mouse exposed to AMF (SH, LL, LH, HL and HH) using fiber optic temperature probes [12,39].

NIH-PA Author Manuscript

NIH-PA Author Manuscript

NIH-PA Author Manuscript

Euthanasia & terminal specimen collection

Terminal blood was collected by cardiocentesis from mice deeply anesthetized by isoflurane anesthesia. Euthanasia was performed by CO_2 exposure for 5–10 min, followed by cervical dislocation. Entire spleens and liver lobes were collected and fixed by immersion in 10% neutral buffered formalin.

Clinical chemistry

Serum was separated from fresh clotted whole blood by centrifugation (5000 rpm for 10 min). Serum alanine aminotransferase (ALT), aspartate aminotransferase (AST), and lactate dehydrogenase (LDH) activity were measured spectrophotometrically using a VetACE™ automated clinical chemistry instrument (Alfa Wassermann Inc., NJ, USA).

Histopathology

Formalin-fixed liver and spleen sections were prepared and stained with hematoxylin and eosin. Perls' reaction was used to qualitatively confirm the presence of ferric (Fe^{3+}). Slides were examined by two pathologists and evaluated for necrosis and pigment.

Mass spectrometry

Half of each liver and spleen was processed for measuring the total iron content by inductively coupled plasma mass spectrometry. Each tissue sample was transferred to a 7-ml Teflon microwave digestion vessel (Savillex Corporation, MN, USA), to which 1 ml of optima-grade HNO_3 (Fisher Scientific, MD, USA) was added. The vessel was sealed and placed into a 55-ml Teflon microwave digestion vessel (CEM Corporation, NC, USA), to which 10 ml of ultra-pure H_2O (Millipore Corporation, MA, USA) was added. The 55-ml vessel was sealed and assembled according to the manufacturer's protocol. The assembly was then placed in a MARS5 Xpress microwave (CEM Corporation), where the tissue samples were digested using the following single-stage ramp-to-temperature microwave method: 15 min ramp to 130°C, with a hold of 30 min.

After cooling, each sample was removed from the microwave and diluted: 35 µl of sample digest and 300 µl of HNO_3 were added to 14.665 ml of ultra-pure H_2O to achieve a final HNO_3 concentration of 2% w/v. Scandium (CPI International, CA, USA) was added to a final concentration of 50 µg/l as an internal standard to monitor instrument drift during analysis. For every batch of 20 tissue samples, three samples of Seronorm™ Trace Elements Whole Blood (Sero AS, Billingstad, Norway) and four reagent blanks (for quality control) were digested and analyzed.

The total iron content of the tissue samples was measured using an Agilent 7500ce inductively coupled plasma mass spectrometry (Agilent Technologies, CA, USA). Each measurement was blank-corrected using the average iron value of the reagent blanks, multiplied by the dilution factor, and adjusted based upon the recovery of iron from Seronorm. An eight-point calibration curve (0, 1, 5, 10, 50, 100, 500 and 1000 µg/l) was obtained. The analytical limit of detection was calculated by multiplying the standard deviation of the lowest detectable calibration standard (1 µg/l) by three. For samples with

NIH-PA Author Manuscript

NIH-PA Author Manuscript

NIH-PA Author Manuscript

values below the analytical limit of detection, one-half of the limit of detection was substituted.

Results

Rectal temperature of the mice

During AMF exposure, the authors measured the rectal temperature of each mouse, which indicates the degree of systemic heating the mouse experiences. Systemic heating is in contrast to localized heating from SPIO deposited in, for example, the liver and spleen, which was not measured. However, the authors hypothesized that detectable and possibly dangerous systemic overheating will result from significant localized organ heating by nanoparticle deposits in organs, such as the liver and spleen, as blood carries heat away from these organs and redistributes it throughout the body [39,40].

The mean maximum rectal temperature was 37.5 ± 0.3°C in the control group that received saline injections and high-amplitude AMF (SH); 39.4 ± 0.3°C in group LL; 40.6 ± 0.8°C in group LH; 38.4 ± 0.9°C in group HL; and 41.4 ± 1.1°C in group HH (Tables 1 & 2; Figure 3). Two of the three mice receiving the combined high dose (i.e., high-dose SPIO nanoparticles followed by high-amplitude AMF [group HH]), died during AMF exposure. In one of the HH mice that died, light skin damage was observed in the upper left quadrant of the abdomen (Tables 1 & 2; Figure 3). This nonspecific heating potentially arose from two sources: the energy deposited by heating nanoparticles and; inductive tissue heating or production of eddy currents. Comparison of mean rectal temperature obtained for each group that received combined SPIO and AMF with that obtained in the AMF control (no SPIO) group suggests that the temperature rise due to nonspecific deposition from eddy currents from AMF exposure alone was limited. This suggests that a significant portion (or all) of the observed elevated temperature in the SPIO + AMF groups was attributable to nanoparticle heating.

The rectal temperature data for mice in the SH group (i.e., mice that received saline injections [no nanoparticles] and high-amplitude AMF) demonstrate nominal heating from AMF exposure, with 37.5 ± 0.3°C, or a $\Delta(T_{max} - T_{water\ shield})$ of 0.5 ± 0.3°C. The authors note that the temperatures measured in the SH cohort of mice at high-amplitude AMF reported here are significantly lower than those previously measured in mice exposed to similar high-amplitude AMF conditions [28,40,41]. The authors speculate that this difference resulted from their use of a unique solenoid and shielding configuration [39,40]; however, this was not the focus of the current study.

By contrast, mice from the LH group (i.e., mice that received low-dose SPIO and high-amplitude AMF) had a higher mean maximum temperature of 40.6 ± 0.8°C with a $\Delta(T_{max} - T_{water\ shield})$ of 3.6 ± 0.8°C (group LH), and mice from group HH, (i.e., mice that received high-dose SPIO and high-amplitude AMF) had the highest mean maximum temperature, at 41.4 ± 1.1°C with a $\Delta(T_{max} - T_{water\ shield})$ of 4.4 ± 1.1°C. Thus, energy deposited by heating nanoparticles contributed to the heat deposition observed, suggesting limited nonspecific power deposition from AMF exposure.

NIH-PA Author Manuscript

NIH-PA Author Manuscript

NIH-PA Author Manuscript

Finally, two-sample *t*-tests (for unequal variance or Welch's *t*-test) results indicated that rectal temperature differences between low- (LL and HL) and high-field (LH and HH) cohorts were statistically significant, with a p-value of 0.002. This contrasts with rectal temperature differences between low- (LL and LH) and high-dose SPIO (HL and HH) cohorts, which were not statistically significant, with a p-value of 0.69. When compared with the control (i.e., the SH cohort) rectal temperature differences were statistically significant for both LH and HH groups, with p-values of 0.0264 and 0.029, respectively.

Clinical chemistry

Serum AST activity was elevated only in mice treated with high-dose SPIO nanoparticles followed by high-amplitude AMF (group HH). On the other hand, ALT activity was elevated in both HH and LH groups, suggesting hepatocyte injury at high-amplitude AMF, before frank necrosis, even with low doses of nanoparticles. Serum LDH activity was elevated in the H0, HL, HH, LL and LH groups, and was highest in specimens with obvious hemolysis, consistent with the presence of this enzyme in erythrocytes (five- or 20-times higher than the maximum clinical dose of iron formulations), independent of AMF exposure (Table 3).

Histopathology

Liver and spleen were assessed semiquantitatively and scored for necrosis and amounts of brown–black pigment, which indicated iron deposition. The presence of (ferric) iron, including ferric iron from both nanoparticles (ferric oxide crystals) and hemolysis, was confirmed with Perls' reaction. In the liver, particulate pigment was primarily parasinusoidal and intracellular, consistent with deposition in Kupffer cells, with only scattered particulate pigment identified in hepatocytes. In the spleen, the pigment was consistently intracellular, primarily in red pulp areas, suggesting that the nanoparticles had accumulated in macrophages. Semiquantitative scoring ranged from 0 to 4, with 0 indicating no observable pigment and 4 indicating highest pigment deposition. Mice treated with low doses of SPIO nanoparticles and high-amplitude AMF (group LH) had liver pigment scores of 1.0 ± 0.0 and a mean score of 1.3 ± 0.6 in the spleen (Table 4), with mild necrosis in both tissues (Figure 4). All mice in this group survived exposure.

Mice treated with high doses of SPIO nanoparticles and high-amplitude AMF (group HH) experienced significant mortality (two out of three or 66%). This group had mean pigment scores of 2.7 ± 1.2 in the liver and 2.0 ± 1.7 in the spleen, but no observable necrosis. The absence of necrosis was attributed to acute death of most mice in this group during AMF exposure. The presence of intravascular erythrocyte ghosts, or lysed erythrocytes, suggest that hemolysis (or hyperthermia) may be proximate contributors to acute death in these cases. Hemolysis also was noted in serum specimens from HH groups (Figure 4).

In addition, intravascular pigments in group HH suggest that heating due to treatment with high-dose SPIO followed by high-amplitude AMF can lead to loss of nanoparticles into the systemic circulation and may result from intravascular hemolysis.

NIH-PA Author Manuscript

NIH-PA Author Manuscript

NIH-PA Author Manuscript

Iron measurements from mass spectrometry—Measurements of the total iron content of tissues help to correlate thermal damage with injected iron dose. Overall, higher measured total iron content of tissues obtained from mass spectrometry corresponded with higher iron deposition scores from histology (Tables 4–7).

Further comparison of total iron content among high-dose SPIO (groups H0, HL and HH), low-dose SPIO (groups LL and LH), and control groups (groups S0 and SH) indicates statistically significant results for the liver but not for the spleen. This indicates that the liver is the most likely site for nonspecific deposition of these SPIO (i.e., dextran–iron oxide nanoparticle suspensions) a finding that is consistent with previously reported results (Tables 5 & 6) [12–15,23,25–27,29,37,41].

Dosimetry—The total heat (energy) deposited (THD) in the organs measured in joules per gram of tissue [25], was calculated using the SLP of the iron particles at each AMF amplitude studied and a mean iron concentration in the liver and spleen (obtained from mass spectrometry). THD is thus:

$$THD = (M)*(SLP)*1800\ s$$

where M is the mass concentration of iron in the liver or spleen (grams iron/grams organ) obtained from mass spectrometry; SLP is the measured power loss, or produced heat (W/g iron), and 1800 s (i.e., 30 min) is the total duration of exposure. Group LL had estimated THDs of 2770 J/g liver and 2880 J/g spleen; group LH had THDs of 3810 J/g liver and 8040 J/g spleen; group HL had THDs of 8050 J/g liver and 5380 J/g spleen, and group HH had THDs of 8870 J/g liver and 17,710 J/g spleen.

Discussion

Understanding the potential for toxicity that results from magnetic iron oxide nanoparticle-based therapies is vital to the design and development of magnetic fluid hyperthermia-based treatments for cancer. In this particular case, the problem is twofold as toxicity may arise from: the nanoparticle formulation (i.e., response to the injected material without any further activation); and inadvertent or inappropriate activation (heating) of particles that accumulate in normal and nontargeted tissues. Certainly, both sources of toxicity may manifest different symptoms, yet they share a common source – both arise from a lack of specificity in targeting the cancer and instead inadvertently target the host immune system. This is true even for ‘targeted’ nanoparticle formulations intended for systemic delivery to treat widely disseminated or occult disease. In this pilot study, the authors provide initial data with mice in which they determined the potential for damage to tissues by magnetically induced hyperthermia from SPIO nanoparticles injected systemically and activated by AMF exposure. Potential cellular damage from exposing iron oxides to magnetic forces has been previously studied in high-field MRI systems, which indicate that magnetic forces on endogenous iron oxide particles are unlikely to disrupt normal cellular function even at 9.4 telsa [42]. However, the potential for thermal damage that may be caused by SPIO in thermoablative procedures remains unexplored because thermoablative procedures use alternating magnetic fields (as opposed to static, super-saturating fields in MRI) and because

NIH-PA Author Manuscript

NIH-PA Author Manuscript

NIH-PA Author Manuscript

thermoablative procedures may employ high-intensity alternating fields that stimulate more heating by the particles.

SPIO nanoparticle dose calculation

Dextran-coated iron oxide particles are often used as supplemental iron therapy, as either an alternative or an adjunct to epoetin therapy for iron-deficient patients [43]. For such clinical uses, the patients are rarely (intentionally) exposed to high-amplitude AMF, and the iron oxides typically lack ferromagnetic properties and therefore do not heat significantly when exposed to AMF. The author and colleagues assume that this clinical experience with dextran–iron oxide formulations can inform decisions relating to general tolerance of parenteral dextran–iron oxide suspensions.

Assuming that the maximum tolerated dose of the clinical-grade nonferromagnetic dextraniron–oxide nanoparticles applies to the SPIO particles used in this study, they could estimate a relevant equivalent maximum dose for the mice described in this study. For humans, the maximum dose for a single iv. administration of clinically approved dextran–iron is approximately 1000 mg iv. iron per person [43]. Assuming a mass of 75 kg for a person and 25 g for a mouse, this dose is equivalent to approximately 0.33 mg iv. iron per mouse. Since the iron content of SPIO particles was 6 mg/ml, this is equivalent to 0.055 ml of SPIO injections. In this study, the authors injected 1.2 ml of SPIO nanoparticles (i.e., 7.2 mg iron) per mouse in the high-dose groups (H0, HL and HH) and 0.275 ml of SPIO nanoparticles (i.e., 1.65 mg of iron) per mouse in the low-dose groups (LL and LH). Consequently, the authors evaluated (iron) doses that are about five- and 20-times higher than the expected therapeutic (iron) dose for humans. The objective of this study was to assess the potential for organ-specific thermal damage in mice due to the heating of systemically delivered nanoparticles. Thus, the clinically relevant quantity here may rather be the total heat energy exposure, which is mediated by the iron. Owing to the fact that the SPIO nanoparticles used in this study have modest SLP, the aforementioned objective necessitates the use of higher-than-clinical (iron) doses. Any organ-specific thermal damage discovered in this study justifies further and complete toxicologic evaluations, and serves as a cautionary note to the pursuit of high SLP (efficiently heating) formulations that can damage tissues at much lower doses.

In this study, the authors found that magnetically induced hyperthermia resulting from a high injected dose of nanoparticles significantly elevated rectal temperatures and serum AST, ALT and LDH activity in mice, and caused liver and spleen necrosis, and – in extreme cases – death.

Mice treated with low-dose SPIO nanoparticles followed by low-amplitude AMF (group LL) suffered no discernable adverse effects; however, mice exposed to low-dose SPIO nanoparticles followed by high-amplitude AMF (group LH) had elevated rectal temperatures, elevated ALT, and tissue necrosis in the liver and spleen.

Elevated core temperatures indicate systemic hyperthermia that can lead to widespread tissue and vessel damage.

NIH-PA Author Manuscript

NIH-PA Author Manuscript

NIH-PA Author Manuscript

Despite these adverse effects, all three mice from group LH survived, suggesting that the damage was transient and perhaps clinically irrelevant. Mice treated with high doses of SPIO nanoparticles followed by high-amplitude AMF (HH) experienced elevated rectal temperatures (>41°C), elevated liver enzymes (ALT, AST and LDH) in the blood, and significant mortality. Although necrosis was not observed in these mice, two of the three mice died during AMF treatment.

Elevated rectal temperatures can be due to nonspecific heating from two sources: the energy deposited by heating nanoparticles and; inductive tissue heating, or production of eddy currents [39–41]. The latter source has been well characterized for mice placed in unshielded coils [39,40]. It has been demonstrated, however, that at approximately 150 kHz, mice (without nanoparticle injections) display a modest temperature rise when exposed to field amplitudes below 55 kA/m [39,40], suggesting limited nonspecific power deposition from eddy currents due to AMF exposure alone. Moreover, our current AMF system includes a water shielding system, inserted within the induction coils, which maintains a constant ambient temperature of 37°C for the anesthetized mice, regardless of the existence of eddy currents. Sham control studies demonstrate that ambient temperature within the induction coil quickly equilibrated to 37°C (circulating water shield temperature) within the first 500 s [41]. As a result, the authors' saline controls (group SH, subjected to the AMF system but without nanoparticle injections) had an average rectal temperature of 37.5 ± 0.3°C and did not demonstrate systemic heating (Tables 1 & 2). Thus, they concluded that significant systemic heating of the HH cohort, which received both high dose of nanoparticles and high AMF, must have occurred from nanoparticles. It would be very interesting to visualize temperature distribution during treatment, which is in fact a future direction of research for their group. Unfortunately, due to current technological limitations, temperature probes remain the only thermometric device (nonmetal) that is compatible with their AMF system. As such, visualizing temperature distribution using these probes is invasive and introduces risk to both experimental design and the animals, and limits the value and amount of data they can obtain. As their study aims to be a cursory examination of potential thermal toxicity in normal tissues, it should be noted that intraorgan temperatures within the liver and spleen (which would require intraoperative procedures) were not measured for this study. They believe that tissue histology is sufficient demonstration of local (damaging) heat deposition. Thus, intraorgan temperature within the liver and spleen (which would require intraoperative procedures, with added technical challenges and potential complications) were considered unnecessary for this study only and were not measured. Future studies would benefit from such measurement, and a more complete toxicity study in the authors' subsequent efforts will require such measurements, which could be correlated with nanoparticle dose per mouse.

Noninvasive imaging of nanoparticle distribution, including the use of MRI, optical techniques, x-rays and computed tomography, may also be beneficial in future studies, especially for the development and monitoring of magnetic iron oxide nanoparticles as theragnostic agents [18–24,44,45]. Magnetic iron oxide nanoparticles are considered potentially strong candidates for theragnostic (combined imaging and therapy) applications, including as platforms for drug delivery on demand because of their inherent imaging contrast (MRI) and ability to heat when exposed to AMF.

NIH-PA Author Manuscript

NIH-PA Author Manuscript

NIH-PA Author Manuscript

Nevertheless, it should be noted that the THD in the organs is significant and ranges from approximately 3000 J/g organ in group LL to as much as 18,000 J/g spleen in group HH. Moreover, rectal temperature differences were significant for both LH ($p = 0.006$) and HH ($p = 0.02$) groups, when compared with the SH control group. These calculations only estimate the THD. In normally functioning organs and tissues, heat deposited leads to an intratissue temperature rise that is offset by radiative and convective (blood flow) cooling processes. Often a temperature rise will induce a thermo-regulatory response, such as vasodilation that increases the organ or tissue cooling capacity. In this study, the authors estimate the theoretical total energy produced in the tissue from available data and correlate this estimate with the observed end points. Further study that correlates the net energy deposited (i.e., accounts for cooling capacity) with intratissue temperature and response is warranted. In addition, it is necessary to establish that the 'heat-related' damage is specific to the heat and is not confounded by material-related (i.e., iron) cytotoxicity.

Thus, the authors' data suggest that dextran–SPIO nanoparticles accumulated predominantly in the liver and spleen after iv. administration, consistent with the observations of others [12,22,25]. To their knowledge, their study is the first to provide preliminary data in assessing the potential for adverse effects after exposing mice to AMF following the iv. administration of this type of magnetic nanoparticle suspensions. Considering the accumulation of SPIO nanoparticles in the liver and spleen, they evaluated the iron content of these organs. In general, iron content increases with increasing doses of SPIO nanoparticles, leading to increased total heat energy deposition and tissue destruction. Higher pigment scores from histopathology corresponded with higher iron concentrations obtained by mass spectrometry. The author and colleagues emphasize the need for all future studies to include more comprehensive evaluations of toxicity, which for nanoparticle-mediated hyperthermia applications, incorporates intraorgan temperature data measurements, correlated with energy calculations, and expanded cohorts for different types of hyperthermia-inducing agents.

The iron concentrations in the liver and spleen of mice within a particular treatment group showed wide variation. In the HH group, iron concentrations varied from 3.02 to 210.8 μg Fe/mg dry tissue and from 0.59 to 137.5 μg Fe/mg fresh organ in the spleen; and from 8.13 to 91.81 μg Fe/mg dry tissue and from 2.32 to 49.32 μg Fe/mg fresh organ in the liver. This high degree of variation may have been due to a number of factors, including early death (two out of three mice died during AMF exposure), hemolysis and differences in SPIO clearance rates for individual mice. More importantly, the source of the variation may be biological iron source deposition, given that mass spectrometry does not distinguish between biological or retro-orbitally injected iron. Assuming a blood iron concentration of 545 μg/ml, a blood volume of 5.5 ml/100 g mouse [46,47] and an average bodyweight of 25 g per mouse, the authors estimate that the total blood iron content is 0.75 mg. This estimate is consistent with their measurements of normal endogenous blood iron content, which averaged at 0.44 ± 0.17 μg/mg blood (n=14), or 0.77 ± 0.30 mg total blood iron content (assuming that blood is 7% of the total bodyweight and that the average mouse has a total bodyweight of 25 g). They injected a total dose of 7.2 mg iron in the high-dose mice (groups H0, HL and HH) via retro-orbital injections. The mean total liver iron content in these mice was 28.2 mg, or approximately 21 mg in excess of the injected iron content, suggesting that

NIH-PA Author Manuscript

NIH-PA Author Manuscript

NIH-PA Author Manuscript

the iron content resulted from biological iron deposition. Nevertheless, their data reveal statistical significance when comparing total iron content in the liver among high- versus low-dose cohorts ($p = 0.03$) and among low-dose versus control cohorts ($p = 0.0006$), suggesting that the increase in iron concentration for the SPIO-injected groups cannot be accounted for by endogenous iron content alone. For further validation, future studies should consider alternate methods in specifically measuring the superparamagnetic iron coming from nanoparticles and distinguishing it from endogenous iron.

In addition, heating from a combined high-amplitude AMF exposure with high doses of SPIO nanoparticles can lead to a loss of tissue integrity and thus increased clearance of nanoparticles from the liver into the systemic circulation. This result merits further study to determine SPIO concentration and distribution following exposure to AMF. It is interesting to note that while rectal temperature increase was consistently higher in the HH group, physiological response (as demonstrated by liver enzymes and the degree of thermal damage and necrosis, as determined by histology) can be highly variable. In short, the authors do not know why, but they suspect that it is due to natural variability. They know that a rectal (body core) temperature of 42°C is lethal to mice in nearly 100% of cases. Approaching this (i.e., 40 or 41°C) will cause death in some individuals, depending upon a number of variables. This is the nature of variability (individuality) in biological systems. Furthermore, they may consider that the source of heating – the liver and spleen – may have an effect on the survival statistics. Measured rectal temperatures of the two mice that died represent both the lowest (40.1°C) and the highest (42.2°C) measured temperatures in this group (Table 1). The reason behind this requires further investigation. These initial results highlight the need for comprehensive toxicologic evaluations that include potential toxicity from heating magnetic nanoparticles tissues, and it also indicates the need for a subsequent, more comprehensive study with expanded cohorts for more robust statistical stability.

Finally, as this study demonstrates, nanoparticles capable of producing only modest heat output when compared with other and newer nanoparticle formulations show significant potential for damage at doses that are not acutely toxic from a material-property perspective [14,24]. The dextran–SPIO formulation used in this study has a specific biodistribution profile, resulting in nonspecific deposition in the liver and spleen. Magnetic nanoparticles having different coating material combinations may deposit in different organs and to varying degress, thus altering or modulating the potential toxicity from AMF heating. In recent years, research in nanoparticle-based thermoablation has focused primarily on the design and development of particles with higher SLP. This study however, suggests that high SLP particles may in fact induce higher systemic damage, and research in this direction will have to be carefully balanced with higher specificity in targeting nanoparticles to the tumor site. This study, which focuses on thermal effects of nontargeted nanoparticles, may potentially serve as a reference for future studies of delivery specificity with targeted nanoparticles. In other words, given the same nanoparticle formulation, the authors can find an estimate of delivery specificity based on thermal toxicity data from both targeted and nontargeted particles.

NIH-PA Author Manuscript

NIH-PA Author Manuscript

NIH-PA Author Manuscript

Conclusion

To summarize, this study demonstrates a potential for inadvertent tissue damage from nanoparticles having a modest heat output that were systemically injected into mice, sequestered in sufficient concentration and subsequently heated by AMF. Dextran–SPIO nanoparticles typically deposit in the liver and spleen, making these the sites of potential toxicity for this type of nanoparticle. Other nanoparticle material-coating combinations may result in different distribution profiles, leading to different results. This pilot study raises the concern that toxicologic evaluations of different nanoparticle formulations must include all aspects of their intended (and perhaps unintended) use that goes beyond the traditional assessments of material, protein and cell interactions and attendant cytotoxicity, biodistribution and immune-system response, among others. The authors emphasize the need for a more comprehensive study of toxicity, which for nanoparticle-mediated hyperthermia applications, incorporates intraorgan temperature data measurements, correlated with energy calculations, and expanded cohorts for different types of hyperthermia-inducing agents.

Future perspective

The potential of magnetic iron oxide nanoparticle hyperthermia as a tool for cancer therapy has received considerable attention. Despite many unsuccessful attempts, there is renewed interest due to the development of novel nanoparticle formulations that are able to deliver high-heat payloads in substantially smaller doses than was possible in previous decades. This study however, suggests that particles having a high SLP may in fact induce higher systemic damage, and further research in this direction will have to be carefully balanced with higher specificity in targeting nanoparticles to the tumor site. In fact, clinical success for hyperthermia as an adjuvant cancer therapy for widespread (systemic) disease can only be realized if two conditions are met:

- Specific accumulation in cancer tissue is significantly enhanced;
- Nonspecific uptake of the nanoparticles is minimized or significantly reduced by nontargeted organs and tissues following systemic delivery.

Current formulations have not yet demonstrated substantial success in either category, yet there is a growing realization that this should be the focus of research and development efforts in the coming decade. Further effort in the coming years should also be directed towards developing toxicology assays that are specific for nanoparticle formulations. As this study demonstrates, nanoparticles capable of producing only modest heat output when compared with other and newer nanoparticle formulations [14,24], have significant potential for damage at doses that are not acutely toxic from a material-property perspective. Further and full characterization of the toxic effects of hyperthermia-inducing nanoparticles, including both passive (material-induced) and active (energy-induced) toxicity, will be necessary, particularly for multifunctional nanoscale therapeutic devices.

NIH-PA Author Manuscript

NIH-PA Author Manuscript

NIH-PA Author Manuscript

Acknowledgments

The authors wish to thank G Holzhüter of the University of Rostock, Germany for transmission electron microscopy imaging and characterization, and acknowledge assistance from M Jones in the preparation of this manuscript.

This research was supported by an award from the Prostate Cancer Foundation (CA, USA) and Safeway STAR Program (CA, USA). ICP-MS analysis was supported, in part, by the Maryland Cigarette Restitution Fund Program at the Johns Hopkins Bloomberg School of Public Health and the NIEHS Center P30 E00319.

References

Papers of special note have been highlighted as:

■ of interest

■■ of considerable interest

1. Dewhirst MW, Viglianti BL, Lora-Michiels M, Hanson M, Hoopes PJ. Basic principles of thermal dosimetry and thermal thresholds for tissue damage from hyperthermia. Int. J. Hyperthermia. 2003; 19(3):267–294. [PubMed: 12745972] ■ Summarizes hyperthermia data and thermal dosimetry providing fundamental information about hyperthermia.
2. Horsman MR, Overgaard J. Hyperthermia: a potent enhancer of radiotherapy. Clin. Oncol. (R. Coll. Radiol.). 2007; 19(6):418–426. [PubMed: 17493790]
3. Myerson RJ, Roti Roti JL, Moros EG, Straube WL, Xu M. Modelling heat-induced radiosensitization: clinical implications. Int. J Hyperthermia. 2004; 20(2):201–212. [PubMed: 15195514]
4. van der Zee J. Heating the patient: a promising approach? Ann. Oncol. 2002; 13(8):1173–1184. [PubMed: 12181239]
5. Krawczyk PM, Eppink B, Essers J, et al. Mild hyperthermia inhibits homologous recombination, induces *BRCA2*degradation, and sensitizes cancer cells to poly (ADPribose) polymerase-1 inhibition. Proc. Natl Acad. Sci. 2011; 108(24):9851–9856. [PubMed: 21555554] ■■Recent data demonstrating that very mild (nonlethal) hyperthermia is a potent radio-sensitizer by abrogating DNA double-strand repair and offers significant motivation for development of heat-based therapies for cancer.
6. Overgaard J, Gonzalez Gonzalez D, Hulshof MC, et al. Hyperthermia as an adjuvant to radiation therapy of recurrent or metastatic malignant melanoma. A multicentre randomized trial by the European Society for Hyperthermic Oncology. Int. J. Hyperthermia. 1996; 12(1):3–20. [PubMed: 8676005]
7. Sneed PK, Stauffer PR, Mcdermott MW, et al. Survival benefit of hyperthermia in a prospective randomized trial of brachytherapy boost +/− hyperthermia for glioblastoma multiforme. Int. J. Radiat. Oncol. Biol. Phys. 1998; 40(2):287–295. [PubMed: 9457811]
8. Valdagni R, Amichetti M. Report of long-term follow-up in a randomized trial comparing radiation therapy and radiation therapy plus hyperthermia to metastatic lymph nodes in stage IV head and neck patients. Int. J. Radiat. Oncol. Biol. Phys. 1994; 28(1):163–169. [PubMed: 8270437]
9. Vernon CC, Hand JW, Field SB, et al. Radiotherapy with or without hyperthermia in the treatment of superficial localized breast cancer: results from five randomized controlled trials. International Collaborative Hyperthermia Group. Int. J. Radiat. Oncol. Biol. Phys. 1996; 35(4):731–744. [PubMed: 8690639]
10. Jones EL, Oleson JR, Prosnitz LR, et al. Randomized trial of hyperthermia and radiation for superficial tumors. J. Clin. Oncol. 2005; 23(13):3079–3085. [PubMed: 15860867]
11. Jones EL, Samulski TV, Dewhirst MW, et al. A pilot Phase II trial of concurrent radiotherapy, chemotherapy, and hyperthermia for locally advanced cervical carcinoma. Cancer. 2003; 98(2): 277–282. [PubMed: 12872345]
12. Denardo SJ, Denardo GL, Miers LA, et al. Development of tumor targeting bioprobes (111In-chimeric L6 monoclonal antibody nanoparticles) for alternating magnetic field cancer therapy.

NIH-PA Author Manuscript

NIH-PA Author Manuscript

NIH-PA Author Manuscript

Clin. Cancer Res. 2005; 11(19 Pt 2):7087s–7092s. [PubMed: 16203807] ■■Antibody-targeted superparamagnetic iron oxide nanoparticles similar to those described in this article were used for therapy in mice. Biodistribution shows significant liver and spleen deposition.

13. Moroz P, Jones SK, Gray BN. Magnetically mediated hyperthermia: current status and future directions. Int. J. Hyperthermia. 2002; 18(4):267–284. [PubMed: 12079583]
14. Natarajan A, Gruettner C, Ivkov R, et al. NanoFerrite particle based radioimmunonanoparticles: binding affinity and *in vivo* pharmacokinetics. Bioconjug. Chem. 2008; 19(6):1211–1218. [PubMed: 18517234] ■■Several antibody-targeted nanoparticle formulations were compared in mouse models of cancer for pharmacokinetics and biodistribution.
15. Pankhurst QA, Connolly J, Jones SK, Dobson J. Applications of magnetic nanoparticles in biomedicine. J. Appl. Phys. 2003; 36:R167–R181. ■ Summarizes the developments in the applications of magnetic nanoparticles in medicine.
16. Creixell M, Bohórquez AC, Torres-Lugo M, Rinaldi C. EGFR-targeted magnetic nanoparticle heaters kill cancer cells without a perceptible temperature rise. ACS Nano. 2011; 5(9):7124–7129. [PubMed: 21838221] ■■Targeted nanoparticle hyperthermia may not conform to traditional dosimetric models (also see [1]).
17. Portilho FA, Estevanato LLC, Miranda-Vilela AL, et al. Investigation of a magnetohyperthermia system efficacy. J. Appl. Phys. 2011; 109:07B307.
18. Amiri H, Mahmoudi M, Lascialfari A. Superparamagnetic colloidal nanocrystal clusters coated with polyethylene fumarate: a possible novel theranostic agent. Nanoscale. 2011; 3(3):1022–1030. [PubMed: 21152576]
19. Banerjee R, Katsenovich Y, Lagos L, Mciintosh M, Zhang X, Li CZ. Nanomedicine: magnetic nanoparticles and their biomedical applications. Curr. Med. Chem. 2010; 17(27):3120–3141. [PubMed: 20629620]
20. Chen B, Wu W, Wang X. Magnetic iron oxide nanoparticles for tumor-targeted therapy. Curr. Cancer Drug Targets. 2011; 11(2):184–189. [PubMed: 21158723]
21. Kumar CS, Mohammad F. Magnetic nanomaterials for hyperthermia-based therapy and controlled drug delivery. Adv. Drug Deliv. Rev. 2011; 63(9):789–808. [PubMed: 21447363]
22. Vigor KL, Kyrtatos PG, Minogue S, et al. Nanoparticles functionalized with recombinant single chain Fv antibody fragments (scFv) for the magnetic resonance imaging of cancer cells. Biomaterials. 2010; 31(6):1307–1315. [PubMed: 19889453]
23. Krishnan KM. Biomedical nanomagnetics: a spin through possibilities in imaging, diagnostics, and therapy. IEEE Trans. Magn. 2010; 46(7):2523–2558. [PubMed: 20930943] ■ Describes the magnetic properties of nanoparticles for therapy and imaging.
24. Pankhurst QA, Thanh NKT, Jones SK, Dobson J. Progress in applications of magnetic nanoparticles in biomedicine. J. Appl. Phys. 2009; 42(22):224001. ■ Recent developments for applications of magnetic nanoparticles in medicine.
25. Denardo SJ, Denardo GL, Natarajan A, et al. Thermal dosimetry predictive of efficacy of 111In-ChL6 nanoparticle AMF-induced thermoablative therapy for human breast cancer in mice. J. Nucl. Med. 2007; 48(3):437–444. [PubMed: 17332622] ■■Describes antibody-targeted (superparamagnetic iron oxide) nanoparticle thermal therapy in mouse models of human cancer. Energy-based dosimetry concepts were developed, as well as a guide for total head dose calculations.
26. Wang YX, Hussain SM, Krestin GP. Superparamagnetic iron oxide contrast agents: physicochemical characteristics and applications in MR imaging. Eur. Radiol. 2001; 11(11):2319–2331. [PubMed: 11702180]
27. Corot C, Robert P, Idee JM, Port M. Recent advances in iron oxide nanocrystal technology for medical imaging. Adv. Drug Deliv. Rev. 2006; 58(14):1471–1504. [PubMed: 17116343]
28. Bordelon D, Cornejo C, Gruttner C, Westphal F, Deweese T, Ivkov R. Magnetic nanoparticle heating efficiency reveals magneto-structural differences when characterized with wide ranging and high amplitude alternating magnetic fields. J. Appl. Phys. 2011; 109(12):124904.
29. Weissleder R, Stark DD, Engelstad BL, et al. Superparamagnetic iron oxide: pharmacokinetics and toxicity. AJR. Am. J. Roentgenol. 1989; 152(1):167–173. [PubMed: 2783272]

NIH-PA Author Manuscript

NIH-PA Author Manuscript

NIH-PA Author Manuscript

30. Moghimi SM, Szebeni J. Stealth liposomes and long circulating nanoparticles: critical issues in pharmacokinetics, opsonization and protein-binding properties. Prog. Lipid Res. 2003; 42:463–478. [PubMed: 14559067]
31. Mahmoudi M, Hosseinkhani H, Hosseinkhani M, et al. Magnetic resonance imaging tracking of stem cells *in vivo* using iron oxide nanoparticles as a tool for the advancement of clinical regenerative medicine. Chem. Rev. 2011; 111(2):253–280. [PubMed: 21077606]
32. Mahmoudi M, Lynch I, Ejtehadi MR, Monopoli MP, Bombelli FB, Laurent S. Protein–nanoparticle interactions: opportunities and challenges. Chem. Rev. 2011; 111(9):5610–5637. [PubMed: 21688848] ■■Summarizes protein binding and corona on nanoparticle surfaces, and resulting effects on biodistribution.
33. Maurer-Jones MA, Bantz KC, Love SA, Marquis BJ, Haynes CL. Toxicity of therapeutic nanoparticles. Nanomedicine (Lond.). 2009; 4(2):219–241. [PubMed: 19193187] ■ Describes nanoparticle toxicity.
34. Nel AE, Madler L, Velegol D, et al. Understanding biophysicochemical interactions at the nano-bio interface. Nat. Mater. 2009; 8(7):543–557. [PubMed: 19525947]
35. Institute of Laboratory Animal Resources; Commission on Life Sciences; National Research Council. Guide for the Care and Use of Laboratory Animals. 7th Ed. DC, USA: National Academies Press; 1996.
36. Bordelon D, Goldstein R, Nemkov R, et al. Modified solenoid coil that efficiently produces high amplitude AC magnetic fields with enhanced uniformity for biomedical applications. IEEE Trans. Magn. 2012; 48(1):47–52.
37. Kim JS, Yoon TJ, Yu KN, et al. Toxicity and tissue distribution of magnetic nanoparticles in mice. Toxicol. Sci. 2006; 89(1):338–347. [PubMed: 16237191]
38. Rudershausen S, Grüttner C, Frank M, Teller J, Westphal F. Multifunctional superparamagnetic nanoparticles for life science applications. European Cells Mater. 2002; 3(2):81–83.
39. Ivkov R, Denardo SJ, Daum W, et al. Application of high amplitude alternating magnetic fields for heat induction of nanoparticles localized in cancer. Clin. Cancer Res. 2005; 11(19 Pt 2):7093s–7103s. [PubMed: 16203808]
40. Trakic A, Liu F, Crozier S. Transient temperature rise in a mouse due to low-frequency regional hyperthermia. Phys. Med. Biol. 2006; 51(7):1673–1691. [PubMed: 16552097]
41. Ivkov R, Mallipudi R, Kumar A, Deweese T. AMF shielding reduces nonspecific tissue heating for magnetic nanoparticle therapy. Int. J. Rad. Onc. Biol. Phys. 2010; 78(3 Suppl):S658.
42. Dobson J, Bowtell R, Garcia-Prieto A, Pankhurst Q. Safety implications of high-field MRI: actuation of endogenous magnetic iron oxides in the human body. PLoS ONE. 2009; 4(5):E5431. [PubMed: 19412550]
43. Macdougall IC. Strategies for iron supplementation: oral versus intravenous. Kidney Int. Suppl. 1999; 69:S61–S66. [PubMed: 10084288]
44. Huang H, Delikanli S, Zeng H, Ferkey DM, Pralle A. Remote control of ion channels and neurons through magnetic-field heating of nanoparticles. Nat. Nano. 2010; 5(8):602–606.
45. Lee S, Xie J, Chen X. Peptide-based probes for targeted molecular imaging. Biochemistry. 2010; 49(7):1364–1376. [PubMed: 20102226]
46. Bernstein, SE. Physiological Characteristics. In: Green, EL., editor. Biology of the Laboratory Mouse. NY, USA: Dover Publications; 1966.
47. Modak AT, Stavinoha WB, Frazer JW, Deam AP. Estimation of blood content in the mouse brain by measurement of iron. J. Pharmacol. Methods. 1978; 1(3):247–253.

NIH-PA Author Manuscript

NIH-PA Author Manuscript

NIH-PA Author Manuscript

Executive summary

Background

- Understanding the potential for magnetic iron oxide nanoparticles to cause bystander tissue damage is vital to the design and development of magnetic fluid hyperthermia-based treatments for cancer. This is especially true for the development of ‘targeted’ nanoparticle formulations intended for systemic delivery to treat widely disseminated or occult disease.
- The potential for thermal damage due to superparamagnetic iron oxide (SPIO) nanoparticles used in thermoablative procedures remains only a little explored.

Materials & methods

- In this study, the authors adopted (particle-based) dosages at five- and 20-times higher than clinically tolerable ranges, as measured by iron concentration.
- For magnetic fields, they used a system at 140–160 kHz with 24 kA/m and 60 kA/m, equivalent to four- and nine-times higher than the clinical magnetic field limit for peripheral tissue heating, respectively.
- These dosages and magnetic field parameters were chosen to mimic the heating potential of novel high-heating formulations that are the current focus of research, and to assess the potential for damage to normal tissue by heat.

Results

- The specific formulations of SPIO nanoparticles that were used accumulated predominantly in the liver and spleen after intravenous administration, consistent with the observations of others.
- Nonspecific heating, as indicated by an increase in rectal temperature, was consistently higher in mice that received both high-dose SPIO nanoparticles and a high-amplitude alternating magnetic field.
- On the other hand, corresponding physiological response (as demonstrated by liver enzymes and the degree of thermal damage and necrosis, as assessed by histology) was highly variable.

Discussion

- While the scope of this study was limited to one particular SPIO formulation, it highlights the need for a more comprehensive study that includes intraorgan temperature data and the use of expanded cohorts and multiple nanoparticle types when assessing the potential therapeutic value of magnetic nanoparticles as hyperthermia agents.

Conclusion & future perspective

NIH-PA Author Manuscript

NIH-PA Author Manuscript

NIH-PA Author Manuscript

- This study demonstrates that a potential for inadvertent tissue damage exists when high-dose SPIO nanoparticles are systemically injected into mice and subsequently heated by alternating magnetic field. These results suggest that significantly more research, including full characterization of the toxic effects of different types of hyperthermia-inducing nanoparticles, is required before implementing magnetic-nanoparticle hyperthermia in the clinic following systemic administration.
- As demonstrated in this study, nanoparticles capable of producing only modest heat output can inadvertently damage normal organs, suggesting that in the future, higher heat output of nanoparticles should be carefully balanced with higher specificity to the target site.

NIH-PA Author Manuscript
NIH-PA Author Manuscript
NIH-PA Author Manuscript

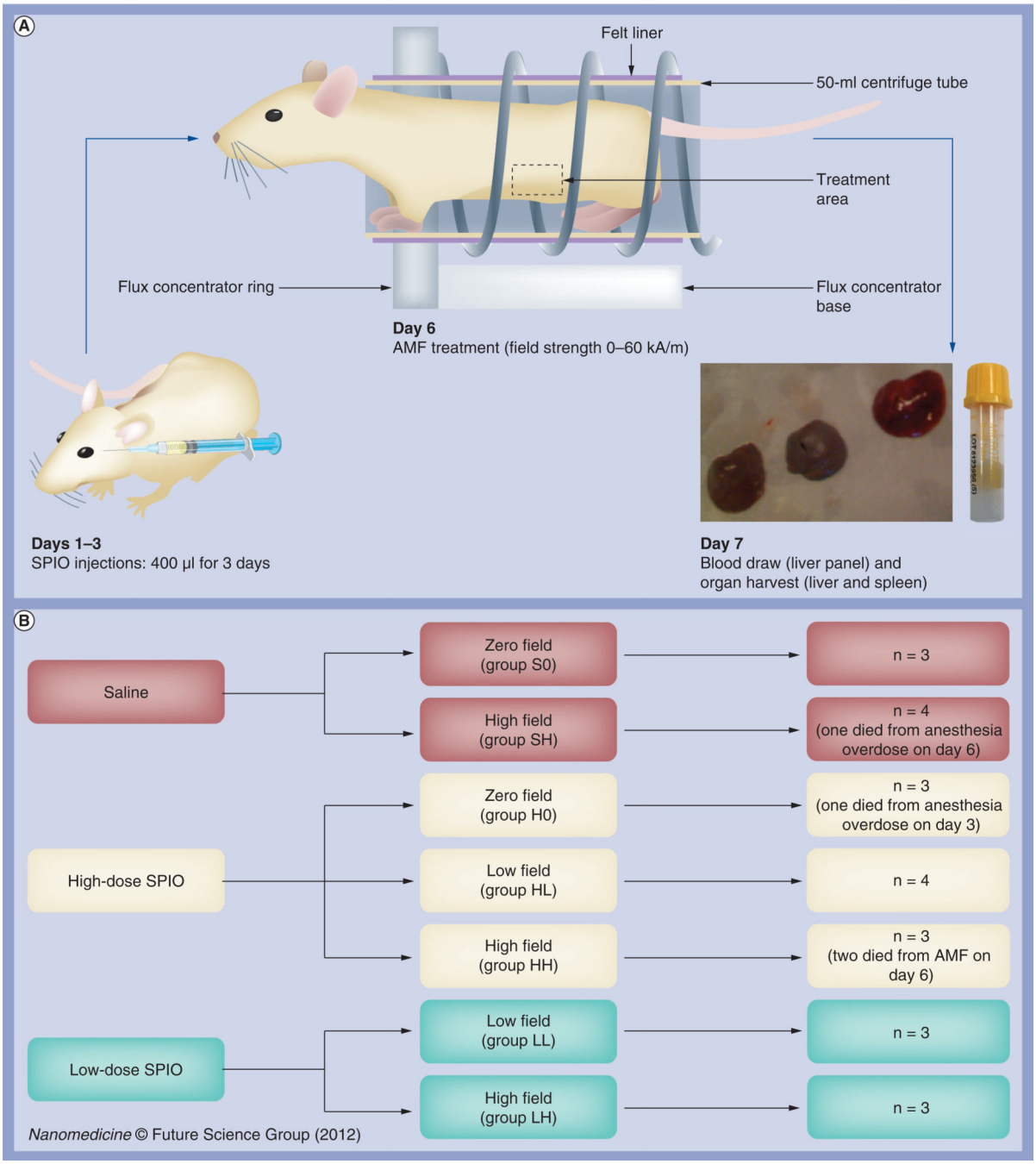

Figure 1. Experimental design

(A) Flow chart of experimental design. Twenty three mice were subjected to daily systemic magnetic dextran–iron oxide injections (at zero, low or high doses) on days 1–3 and exposed to AMF on day 6 (at zero-, low- or high-field strengths). Blood was collected and organs harvested on day 7 for data analysis. **(B)** Mouse group designations. Mice were randomly assigned to seven groups of three to four mice each, including three control groups (S0, SH and H0) and four treatment groups (LL, LH, HL and HH). The first letter of each group designation indicates the dose of nanoparticles injected: saline (S); low-dose (L); or high-

NIH-PA Author Manuscript

NIH-PA Author Manuscript

NIH-PA Author Manuscript

dose (H) SPIO. The second letter of each group designation indicates the field strength for AMF exposure, including zero (0), low (L) and high (H) field. The doses used were 1.65 mg total iron content for low-dose SPIO and 7.2 mg total iron content for high dose, or equivalent to five- and 20-times the maximum tolerated dose for humans. Field strengths used were 24 kA/m for low field and 60 kA/m for high field.

AMF: Alternating magnetic field; SPIO: Superparamagnetic iron oxide.

NIH-PA Author Manuscript
NIH-PA Author Manuscript
NIH-PA Author Manuscript

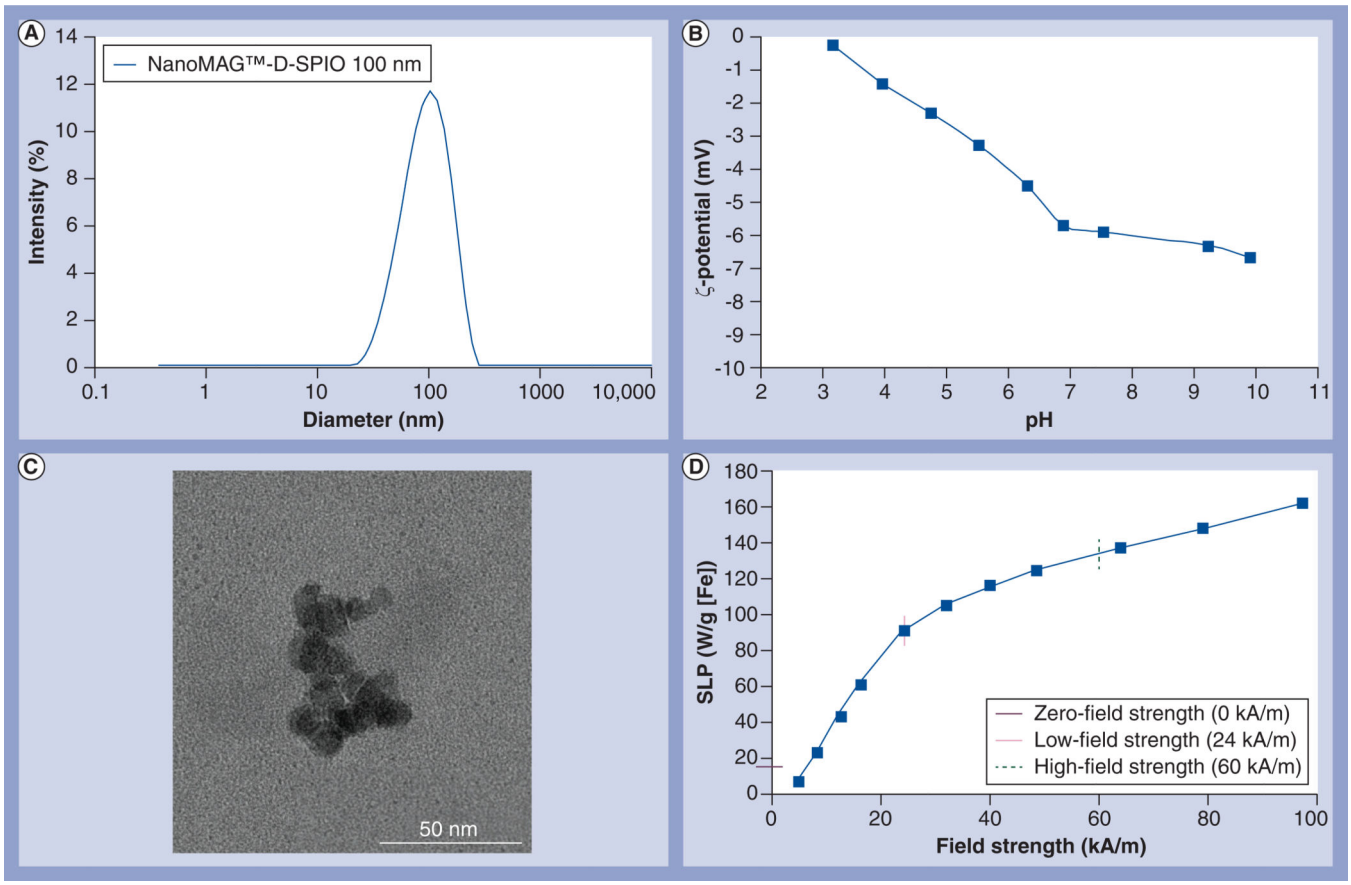

Figure 2. Characterization of superparamagnetic iron oxide nanoparticles

(A) Photon correlation spectroscopy at iron concentrations of 0.2 mg/ml in 0.22-μm-filtered water (z-weighted distribution). **(B)** ζ-potential–pH function. The ζ-potential–pH function of the nanoparticles was measured using a Malvern Zetasizer Nano ZS-90 (Malvern Instruments Ltd, Worcestershire, UK). The nanoparticles have a slightly negative surface charge over pH 3–10 and a surface charge of −6 mV in the neutral pH range. **(C)** Transmission electron microscopy (TEM) image of dextran–SPIO nanoparticles. The TEM image was obtained using an EM 912 TEM at 100 keV. The dextran coating typically is not visible with high-energy electrons (100 keV), which explains the apparently higher hydrodynamic diameter resulting from photon correlation spectroscopy size measurements (100-nm diameter), in comparison with the diameter of the iron oxide core from TEM images (50-nm diameter). **(D)** The amplitude-dependent SLP was estimated by measuring time-dependent heating at several applied amplitude (voltage) values from 4 to 94 kA/m. The SLP was estimated from the slope, $\Delta T/\Delta t$, of the time–temperature curve.
SLP: Specific loss power; SPIO: Superparamagnetic iron oxide.

NIH-PA Author Manuscript

NIH-PA Author Manuscript

NIH-PA Author Manuscript

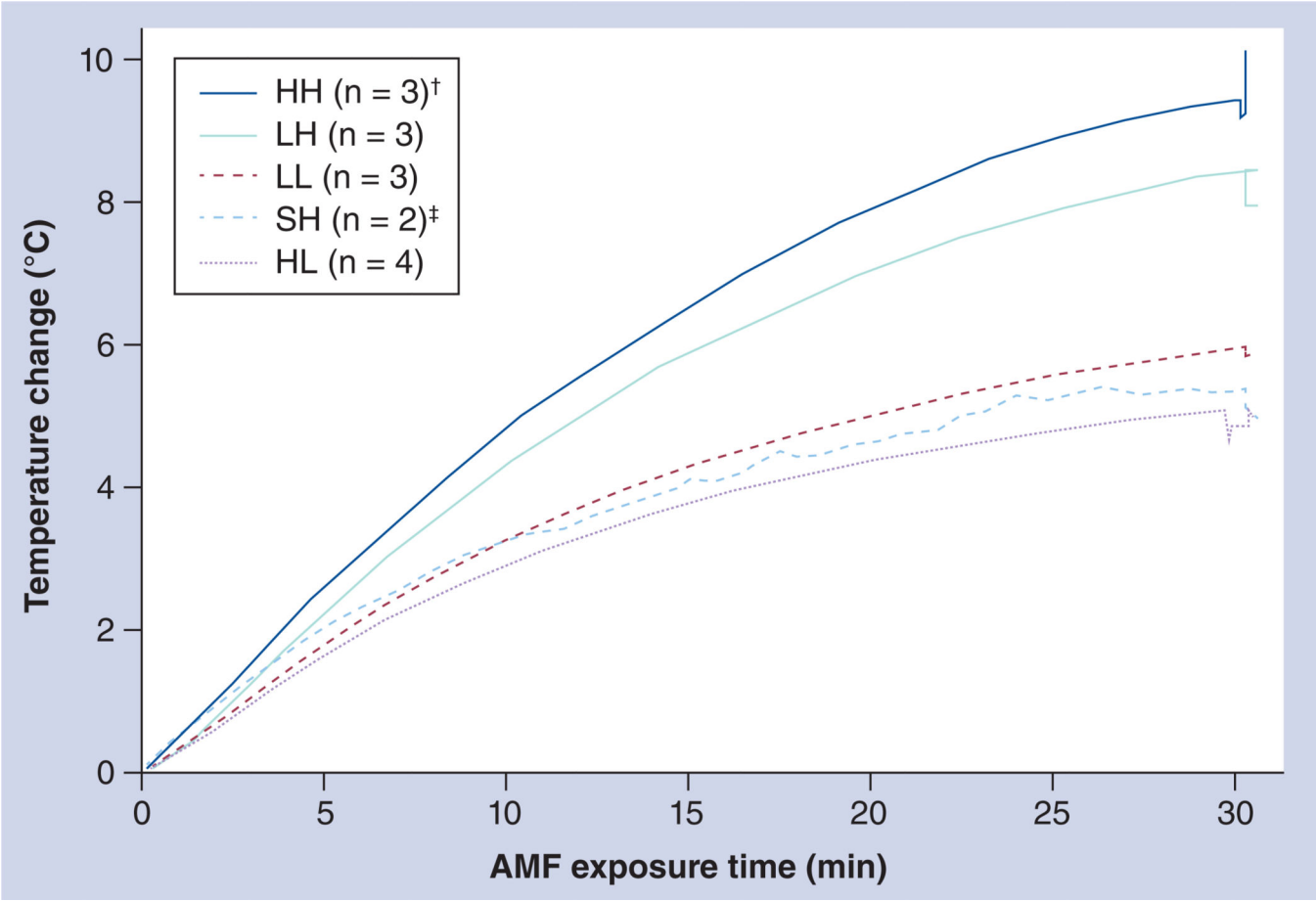

Figure 3. Measured mouse rectal temperatures

Mice were exposed to an AMF at 140–160 kHz for a period of 30 min, during which rectal temperatures were measured. The y-axis illustrates temperature change, which is defined as $T_{max} - T_{initial}$ (averaged maximum rectal temperature – averaged rectal temperature at time point 0) for each mouse group. The first letter of each group designation indicates the dose of nanoparticles injected: saline (S), low-dose (L) or high-dose (H) superparamagnetic iron oxide. The second letter of each group designation indicates the field strength for AMF exposure: low (L) or high (H) field.

†Three mice were assigned to the HH group. Two of these mice perished during AMF exposure.

‡Four mice were used for histological and laboratory analysis for the SH group. However, rectal temperature data were only available for two of these mice (n = 2).

AMF: Alternating magnetic field.

NIH-PA Author Manuscript
NIH-PA Author Manuscript
NIH-PA Author Manuscript

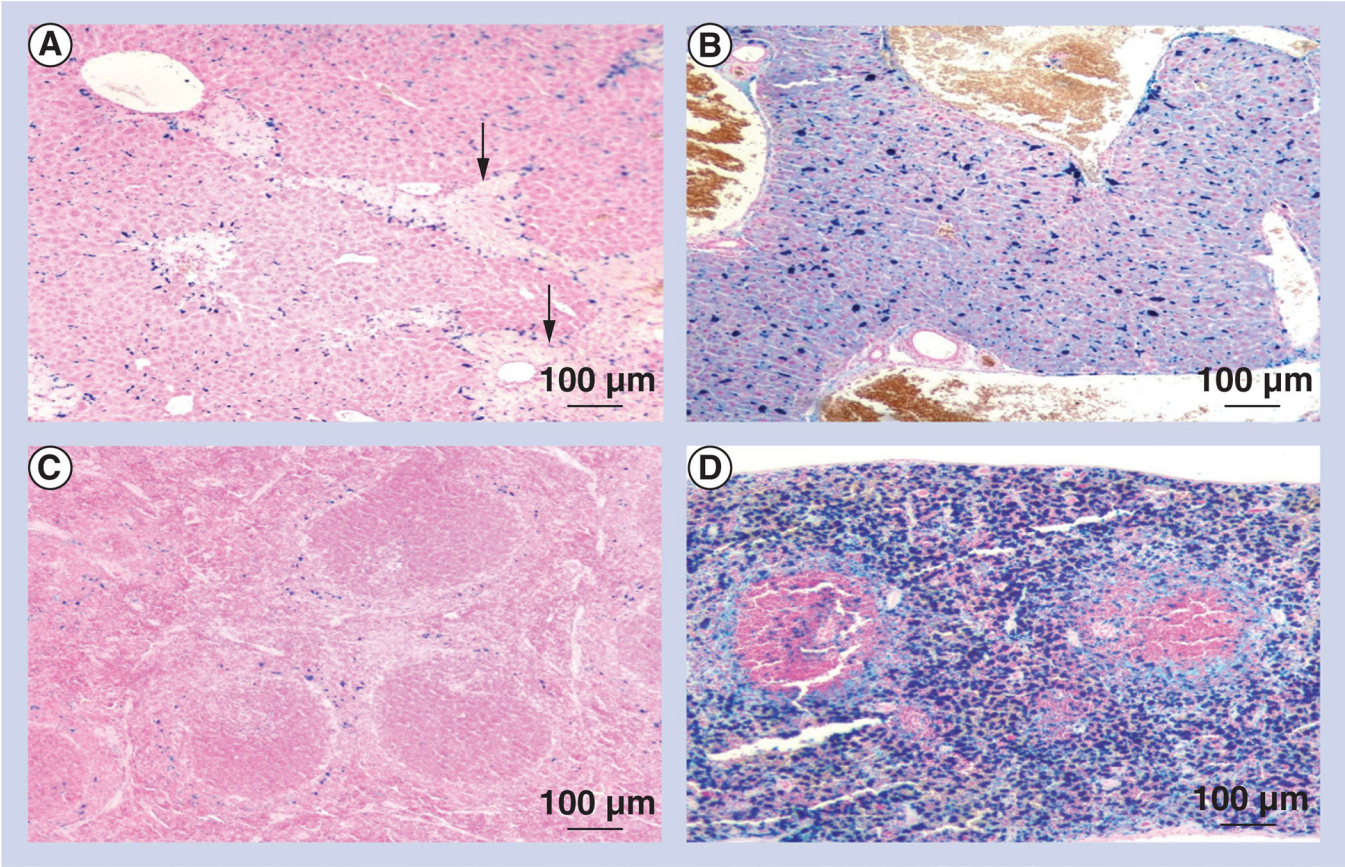

Figure 4. Superparamagnetic iron oxide nanoparticle localization in mice

Mouse livers and spleens were 'stained' with the Perls' Prussian blue reaction, which indicates iron deposition. **(A)** Liver low-dose superparamagnetic iron oxide nanoparticles with high-field alternating magnetic field exposure treatment group; **(B)** liver high-dose superparamagnetic iron oxide nanoparticles with high-field alternating magnetic field exposure treatment group; **(C)** spleen low-dose superparamagnetic iron oxide nanoparticles with high-field alternating magnetic field exposure treatment group; **(D)** spleen high-dose superparamagnetic iron oxide nanoparticles with high-field alternating magnetic field exposure treatment group. Arrows indicate necrosis.

NIH-PA Author Manuscript

NIH-PA Author Manuscript

NIH-PA Author Manuscript

Table 1

Temperature change for different mice groups.

Group designation	Max T (°C)	Max T − $SH_{average}$ (°C)	$T_{max} - T_{water\ shield}$ (°C)
SH.1	37.3	–	0.3
SH.2	37.7	–	0.7
SH.3	_†	–	_†
SH.4	_†	–	_†
SH.average	37.5	–	0.5
SH.SD	0.3	–	0.3
LL.1	39.7	2.2	2.7
LL.2	39.3	1.8	2.3
LL.3	39.2	1.7	2.2
LL.average	39.4	1.9	2.4
LL.SD	0.3	0.3	0.3
LH.1	40.1	2.6	3.1
LH.2	40.1	2.6	3.1
LH.3	41.5	4.0	4.5
LH.average	40.6	3.1	3.6
LH.SD	0.8	0.8	0.8
HL.1	39.7	2.2	2.7
HL.2	38.3	0.8	1.3
HL.3	37.9	0.4	0.9
HL.4	37.6	0.1	0.6
HL.average	38.4	0.9	1.4
HL.SD	0.9	0.9	0.9
HH.1	41.8	4.3	4.8
HH.2 (died)	42.2	4.7	5.2
HH.3 (died)	40.1	2.7	3.1
HH.average	41.4	3.9	4.4
HH.SD	1.1	1.1	1.1

†Temperature data not recorded.

During alternating magnetic field exposure, the authors measured the rectal temperature of each mouse using optical temperature probes. Maximum rectal temperature and changes measured by rectal temperature probes are reported for each mice group. Statistical analysis was based on a two-sample *t*-test of unequal variance. The first letter of each group designation indicates the dose of nanoparticles injected: saline (S), low- (L) or high- (H) dose superparamagnetic iron oxide. The second letter of each group designation indicates the field strength for alternating magnetic field exposure: low (L) or high (H) field.

SD: Standard deviation; T: Temperature.

NIH-PA Author Manuscript

NIH-PA Author Manuscript

NIH-PA Author Manuscript

Table 2

Intergroup comparison for the temperature change of different mice groups.

Group comparison	p-value
Low field (n = 7) vs high (n = 6) field	0.002
Low dose (n = 6) vs high (n = 7) dose	0.69
SH (n = 2) vs LH (n = 3)	0.036
SH (n = 2) vs HH (n = 3)	0.029

Statistical analysis was based on a two-sample *t*-test of unequal variance. The first letter of each group designation indicates the dose of nanoparticles injected: saline (S), low-dose (L) or high-dose (H) superparamagnetic iron oxide. The second letter of each group designation indicates the field strength for alternating magnetic field exposure: high field (H).

NIH-PA Author Manuscript
NIH-PA Author Manuscript
NIH-PA Author Manuscript

Nanomedicine (Lond). Author manuscript; available in PMC 2014 April 18.

Table 3

Clinical chemistry in the blood.

Group	n	AST (U/l)†	ALT (U/l)†	LDH (U/l)†	ALP (U/l)†
S0	3	89 ± 5	59 ± 32	361 ± 105	165 ± 35
SH	2	98 ± 17	48 ± 11	284 ± 54	195 ± 8
LL	3	125 ± 54	36 ± 1	1187 ± 231	112 ± 24
LH	3	181 ± 26	272 ± 216	1623 ± 171	104 ± 6
H0	2	96 ± 40	31 ± 3	862 ± 424	99 ± 25
HL	4	211 ± 204	46 ± 27	984 ± 247	137 ± 34
HH	1	805	114	2227	65

†Results are displayed as mean ± standard deviation.

Serum AST, ALT, LDH and ALP activity were measured spectrophotometrically. The first letter of each group designation indicates the dose of nanoparticles injected: saline (S), low-dose (L) or high-dose (H) superparamagnetic iron oxide. The second letter of each group designation indicates the field strength for alternating magnetic field exposure: zero (0), low (L) or high (H) field.

ALP: Alkaline phosphatase; ALT: Alanine aminotransferase; AST: Aspartate aminotransferase; LDH: Lactate dehydrogenase.

NIH-PA Author Manuscript

NIH-PA Author Manuscript

NIH-PA Author Manuscript

Table 4

Iron deposition scores in the liver and spleen.

Group	Liver (Prussian blue)	Spleen (Prussian blue)
S0	0	0
SH	0	0
LL	1	1
LH	1	1.33
H0	2	2.5
HL	2	2
HH	2.67	2

Slides were prepared and stained with hematoxylin and eosin, and were examined by two pathologists and evaluated for necrosis and pigment. Semiquantitative scoring ranged from 0 to 4, with 0 indicating no observable pigment and 4 indicating highest pigment deposition. The first letter of each group designation indicates the dose of nanoparticles injected: saline (S), low-dose (L) or high-dose (H) superparamagnetic iron oxide. The second letter of each group designation indicates the field strength for alternating magnetic field exposure: zero (0), low (L) or high (H) field.

NIH-PA Author Manuscript

NIH-PA Author Manuscript

NIH-PA Author Manuscript

Table 5

Total iron concentrations in the liver and spleen (dry tissue).

Group	n	Liver; μg Fe/mg dry tissue (± SD)	Spleen; μg Fe/mg dry tissue (± SD)
S0	3	1.8 (0.9)	3.1 (2.5)
SH	4	2.1 (1.9)	3.2 (1.3)
LL	3	17.1 (0.3)	17.8 (14.0)
LH	3	15.7 (3.9)	33.1 (32.3)
H0	3	41.1 (28.0)	36.0 (36.2)
HL	4	49.7 (29.3)	33.2 (24.5)
HH	3	36.5 (47.9)	72.9 (119.4)

Iron concentrations were measured by inductively coupled plasma mass spectrometry. The first letter of each group designation indicates the dose of nanoparticles injected: saline (S), low-dose (L) or high-dose (H) superparamagnetic iron oxide. The second letter of each group designation indicates the field strength for alternating magnetic field exposure: zero (0), low (L) or high (H) field.

SD: Standard deviation.

NIH-PA Author Manuscript

NIH-PA Author Manuscript

NIH-PA Author Manuscript

Table 6

Total iron concentrations in the liver and spleen (wet tissue).

Group	n	Liver; μg Fe/mg wet tissue (± SD)	Spleen; μg Fe/mg wet tissue (± SD)
S0	3	0.6 (0.6)	0.7 (0.1)
SH	4	0.6 (0.6)	0.9 (0.2)
LL	3	6.8 (0.4)	3.37 (1.8)
LH	3	5.3 (2.3)	7.2 (7.7)
H0	3	16.3 (11.8)	9.1 (7.8)
HL	4	20.8 (13.3)	10.9 (7.7)
HH	3	18.9 (26.4)	46.3 (79.0)

Iron concentrations were measured by inductively coupled plasma mass spectrometry. The first letter of each group designation indicates the dose of nanoparticles injected: saline (S), low-dose (L) or high-dose (H) superparamagnetic iron oxide. The second letter of each group designation indicates the field strength for alternating magnetic field exposure: zero (0), low (L) or high (H) field.

SD: Standard deviation.

NIH-PA Author Manuscript

NIH-PA Author Manuscript

NIH-PA Author Manuscript

Table 7

Total iron concentrations in the blood, compared with the liver and spleen iron concentrations of control mice (dry tissue).

Group	Liver (n = 3); μg Fe/mg dry tissue (± SD)	Spleen (n = 3); μg Fe/mg dry tissue (± SD)	Blood (n = 14); μg Fe/mg (± SD)
S0	1.8 (0.9)	3.1 (2.5)	0.44 (1.7)

Iron concentrations were measured by inductively coupled plasma mass spectrometry.

S0: Saline nanoparticles with zero-field alternating magnetic field exposure. SD: Standard deviation.